JACS
JOURNAL OF THE AMERICAN CHEMICAL SOCIETY
Article
pubs.acs.org/JACS

Symmetry-Breaking Charge Transfer in a Zinc Chlorodipyrrin Acceptor for High Open Circuit Voltage Organic Photovoltaics

Andrew N. Bartynski,[†] Mark Gruber,[§] Saptaparna Das,[‡] Sylvie Rangan,[∥] Sonya Mollinger,[⊥] Cong Trinh,[‡] Stephen E. Bradforth,[‡] Koen Vandewal,[⊥,#] Alberto Salleo,[⊥] Robert A. Bartynski,[∥] Wolfgang Bruetting,[§] and Mark E. Thompson*[,†,‡]

[†]Department of Chemical Engineering and [‡]Department of Chemistry, University of Southern California, Los Angeles, California 90089, United States

[§]Institute for Physics, Augsburg University, 86135 Augsburg, Germany

[∥]Department of Physics and Astronomy, Rutgers University, Piscataway, New Jersey 08854, United States

[⊥]Department of Materials Science and Engineering, Stanford University, Palo Alto, California 94305, United States

Supporting Information

ABSTRACT: Low open-circuit voltages significantly limit the power conversion efficiency of organic photovoltaic devices. Typical strategies to enhance the open-circuit voltage involve tuning the HOMO and LUMO positions of the donor (D) and acceptor (A), respectively, to increase the interfacial energy gap or to tailor the donor or acceptor structure at the D/A interface. Here, we present an alternative approach to improve the open-circuit voltage through the use of a zinc chlorodipyrrin, ZCl [bis(dodecachloro-5-mesityldipyrrinato)zinc], as an acceptor, which undergoes symmetry-breaking charge transfer (CT) at the donor/acceptor interface. DBP/ZCl cells exhibit open-circuit voltages of 1.33 V compared to 0.88 V for analogous tetraphenyldibenzoperyflanthrene (DBP)/C_{60}-based devices. Charge transfer state energies measured by Fourier-transform photocurrent spectroscopy and electroluminescence show that C_{60} forms a CT state of 1.45 ± 0.05 eV in a DBP/C_{60}-based organic photovoltaic device, while ZCl as acceptor gives a CT state energy of 1.70 ± 0.05 eV in the corresponding device structure. In the ZCl device this results in an energetic loss between E_{CT} and qV_{OC} of 0.37 eV, substantially less than the 0.6 eV typically observed for organic systems and equal to the recombination losses seen in high-efficiency Si and GaAs devices. The substantial increase in open-circuit voltage and reduction in recombination losses for devices utilizing ZCl demonstrate the great promise of symmetry-breaking charge transfer in organic photovoltaic devices.

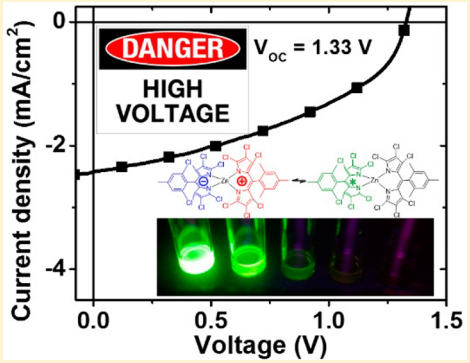

INTRODUCTION

Significant advances have been made in the development of organic photovoltaics (OPVs) as an emerging source of renewable energy, with reported power conversion efficiencies in excess of 10%.[1,2] Nevertheless, the open-circuit voltages (V_{OC}) of organic devices are generally low and serve as a substantial limit to overall device performance. The vast majority of OPVs reported have V_{OC} values below 1 V,[3] and even the best-performing tandem devices often contain subcells that produce nearly identical voltages.[1,2,4] Ultimately, V_{OC} is restricted by the materials chosen for the donor and acceptor. While substantial progress has been made in formulating numerous donors that yield high performance, the corresponding diversity of efficient acceptors is lacking. Fullerenes are without a doubt the most ubiquitous acceptor molecules employed in OPVs, and they have many desirable traits such as their high electron mobility and ability to form efficient heterojunctions with a wide variety of donor materials.[5] However, despite their widespread use, the reported V_{OC} for devices with fullerene acceptors are typically between 0.6 and 0.8 V,[3] with selected systems producing V_{OC} values up to 1.15 V.[6,7] In an attempt to circumvent these issues, a wide variety of non-fullerene acceptor systems have been developed.[8] The highest efficiencies have been achieved by utilizing compounds based on perylene diimides (PDIs)[9] and subphthalocyanines (SubPcs).[10] Large V_{OC} values have been reported for devices with non-fullerene acceptors. For example, Sullivan et al.[11] reported a SubPc/Cl_6SubPc device with a V_{OC} of 1.33 V and Peng et al.[12] utilized a diketopyrrolopyrrole (DPP) acceptor that achieved a V_{OC} of 1.19 V. The high V_{OC} values for these devices are the result of a substantial energy offset between the donor's HOMO and the acceptor's LUMO, limiting light collection predominantly to the blue part of the solar spectrum.

In a system such as an OPV, where charge separation occurs through the transfer of an electron from the donor to the acceptor, V_{OC} is thermodynamically limited by the energetic

Received: January 6, 2015
Published: March 31, 2015

DOI: 10.1021/jacs.5b00146
J. Am. Chem. Soc. 2015, 137, 5397−5405

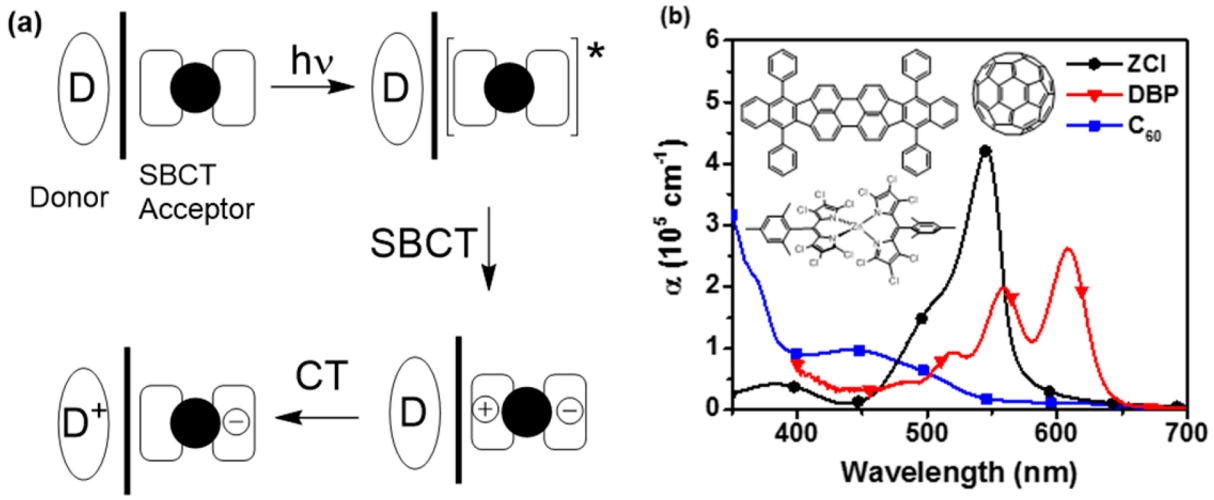

Figure 1. (a) Schematic representation of the charge generation process in an OPV with a conventional donor and a symmetry-breaking charge transfer acceptor. First, an excited state is created through the absorption of a photon. Second, symmetry-breaking charge transfer (SBCT) occurs on the molecule generating an intramolecular charge transfer (ICT) state. Finally, charge transfer (CT) to the donor results in an oxidized donor and reduced acceptor ligand separated by a neutral acceptor ligand. If the excitation takes place in the bulk of the SBCT material, away from the D/A interface, the formed exciton must diffuse to the interface to charge separate. (b) Molecular structures and extinction spectra for DBP, ZCl, and C_{60}.

offset of the HOMO of the donor and the LUMO of the acceptor (E_{DA}). E_{DA} has been argued to be a rather poor predictor of V_{OC}, and it has been shown through spectroscopic and temperature-dependent techniques that the upper bound for V_{OC} is the energy of the ground state to intermolecular charge transfer (CT) state transition (E_{CT}) at the donor/acceptor (D/A) interface.[13−16] E_{CT} is, however, limited by E_{DA}, because in the CT transition an electron is promoted directly from the HOMO of the donor to the LUMO of acceptor. E_{CT} correlates linearly with qV_{OC} with typical energetic losses around 0.6 eV due to recombination. Additional losses between the energy of excitons in the strongly absorbing neat materials and the V_{OC} of a device originate from the offset required to drive formation of the CT state at the D/A interface.

Currently, the largest V_{OC} values are found for devices with the largest E_{DA}. In order to further increase V_{OC} without compromising other important device parameters, i.e., short circuit current, J_{SC}, or fill factor, FF, it would be desirable to minimize the driving force necessary to form the CT state and to reduce the recombination losses to V_{OC}. Symmetry-breaking charge transfer (SBCT) serves as a potential strategy toward this goal. SBCT involves closely associated pairs of identical molecules or compounds composed of two or more identical parts, such as covalently bonded organic dimers or metal complexes with two or more identical ligands. SBCT occurs when an exciton formed initially on one molecule or ligand undergoes intramolecular charge transfer (ICT), leading to a state in which a hole and an electron are localized on different molecules or ligands, with very little coupling between the hole and electron.[17,18] SBCT has been observed in molecular dimers such as 9,9′-bianthryl and in other systems where excitation of the dimer results in an ICT state with an electron on one subunit and a hole on the other.[17−20] Thus, SBCT is an attractive strategy to achieve charge separation with a negligible driving force, directional specificity, and a greatly retarded back-recombination rate. These properties would be beneficial in OPVs, where a lower driving force for charge separation ensures a smaller energy loss due to electron transfer, directionality ensures electrons and holes are positioned toward the appropriate electrode, and retarded back-recombination ensures a high charge separation yield. A simple schematic view of how charge transfer and charge separation involving SBCT could occur at the D/A interface of an OPV is illustrated in Figure 1. SBCT can occur on ultrafast time scales and thus can be kinetically competitive with traditional D/A charge transfer processes, allowing it to participate in the process of charge generation. For example, sub-picosecond charge transfer has been observed in PDI dimers.[21] Trinh et al.'s recent study of SBCT in a series of zinc dipyrrins revealed charge transfer between 1 and 14 ps.[22] The potential advantages of utilizing SBCT to induce charge separation and its unexplored application in OPVs make it an attractive subject for further investigation.

In this work, we study the photophysical and electronic properties of a zinc chlorodipyrrin (ZCl) and utilize it as an acceptor in planar heterojunction OPVs. Transient absorption (TA) studies in a variety of solvents reveal that ZCl undergoes SBCT, evidenced by changes in the excited state dynamics in high dielectric solvents. We probe the LUMO energy of ZCl and C_{60} by inverse photoelectron spectroscopy (IPS), revealing that ZCl has a similar LUMO energy as C_{60} (−4.1 eV), indicating its ability to function as an acceptor. When used in an OPV with tetraphenyldibenzoperyflanthrene (DBP) as donor, ZCl gives markedly higher V_{OC} than the corresponding OPV with C_{60}. Measurements of E_{CT} from Fourier-transform photocurrent spectroscopy and OPV electroluminescence show that C_{60} forms a CT state of 1.45 ± 0.05 eV, while ZCl forms a higher energy CT state at 1.70 ± 0.05 eV with the same donor. This results in a large V_{OC} of 1.33 V for DB/ZCl devices, in contrast with the V_{OC} of 0.88 V for DBP/C_{60}. Comparison of E_{CT} and V_{OC} shows that the energetic losses due to recombination are substantially reduced in ZCl devices. These findings demonstrate exciting possibilities for this class of metallodipyrrins as acceptors and the use of SBCT in OPVs.

■ RESULTS AND DISCUSSION

The absorption spectra in the solid state and the molecular structure of ZCl, C_{60}, and DBP are given in Figure 1. The absorption of DBP is particularly intense, as it orients itself

DOI: 10.1021/jacs.5b00146
J. Am. Chem. Soc. 2015, 137, 5397−5405

largely parallel to the substrate, allowing for strong coupling between the molecular transition dipole and incident electric field, resulting in a maximum extinction greater than 2.5×10^5 cm^{-1} at 610 nm.[23] On the basis of its absorption onset of 650 nm, we estimate an optical gap (E_g) of 1.9 eV for DBP. ZCl exhibits characteristic dipyrrin absorption with a maximum extinction of 4×10^5 cm^{-1} at 545 nm. Compared to C_{60}, ZCl absorbs with almost an order of magnitude greater extinction between 500 and 600 nm. E_g for C_{60} has been determined previously to be 1.85 eV.[24]

Solvent dielectric dependent photophysics is a hallmark of SBCT, where higher-dielectric solvents provide electrostatic stabilization of the resultant CT state. Thus, the polarity of the medium determines the nature of the excited state, i.e., a ligand-localized excited state in nonpolar media and an ICT state in polar media. Recently, we have explored this behavior in a series of homoleptic zinc dipyrrin complexes that undergo SBCT in high-dielectric media.[22] Similar to these complexes, ZCl photoluminesces from a single dipyrrin ligand in low-dielectric solvents and from an ICT state in high-dielectric media, albeit weakly, exemplified by a decrease in quantum yield with increasing solvent dielectric constant (Figure S1, Supporting Information).

Our interpretation of the quantum yield measurements was corroborated with transient absorption (TA) measurements of ZCl in cyclohexane (nonpolar), toluene (weakly polar), and acetonitrile (polar) media. The TA of ZCl in cyclohexane (shown in Figure 2a) shows that the depopulation of the ground state (ground-state bleach between 450 and 550 nm) excited by 520 nm radiation leads to the appearance of the stimulated emission (SE) between 530 and 600 nm[22] and excited-state absorption (ESA) at 360 nm from a localized excited state S_1. At later times, this localized excited state S_1 relaxes to the ground state with an excited state lifetime of ~2.5 ns.[25] Similar to cyclohexane, in a weakly polar medium such as toluene (Figure 2b), SE and ESA from S_1 state appear immediately after the excitation of ZCl. However, within 6 ps, the SE and ESA bands start to disappear with concurrent rising bands at 415 and 545 nm. These new bands are assigned to the ICT state on the basis of similar observations on a series of homoleptic zinc dipyrrin complexes in high-dielectric solvents.[22] As time increases, this ICT state decays to form a T_1 state with a time constant of ~550 ps (long time data with global analysis is shown in the Supporting Information, Figures S2 and S4). In highly polar solvent like acetonitrile, the TA measurements (Supporting Information, Figure S2) show a faster rate (~1.5 ps) of ICT state formation because of higher stabilization of the ICT state in acetonitrile compared to toluene.

To examine whether ICT occurs in the solid state, TA measurements were performed on a film of ZCl dispersed in poly(methyl methacrylate) (PMMA). Similar to toluene, the TA measurements (Figure 2c) show the evolution of similar ICT states (rising bands at 415 and 545 nm), with simultaneous decay of SE and ESA from S_1 state. Interestingly, the generation rate of the ICT state is faster (~0.7 ps), but the amplitude of the bands at 415 and 545 nm are lower in PMMA. The lower production is likely due to a smaller stabilization of the ICT state via solvation due to restricted reorientation in the PMMA matrix. The fast generation rate (0.7–6 ps) of the ICT state in PMMA matrix ($\varepsilon_r \sim 3.5$) and toluene ($\varepsilon_r = 2.38$) shows that moderate polarity, even without solvent reorganization, is sufficient to induce SBCT, resulting in the formation of an ICT

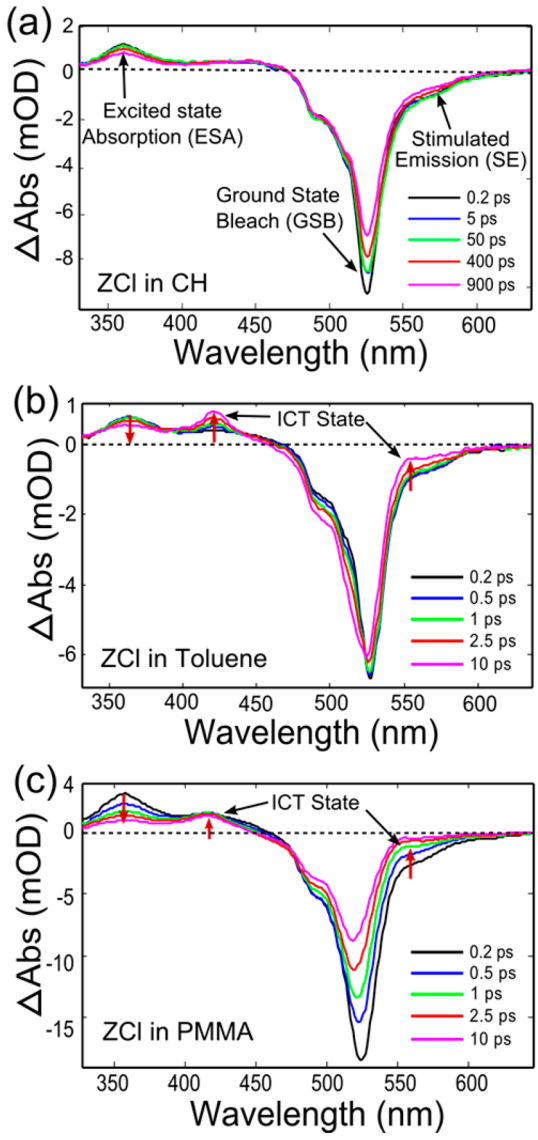

Figure 2. Femtosecond transient absorption of ZCl in cyclohexane (CH) (a), toluene (b), and PMMA (c) at initial delays. An excitation pump fluence of 15 $\mu J/cm^2$ was used for parts a and b and 45 $\mu J/cm^2$ was used for part c. The red arrows highlight the change in the transient spectrum.

state. The presence of this ICT state within a device is expected to markedly affect charge transfer and separation at the D/A interface and thus V_{OC}.

We measured the occupied and unoccupied electronic states of ZCl and compared them to those of C_{60} using ultraviolet photoelectron spectroscopy (UPS) and inverse photoelectron spectroscopy (IPS), respectively. The left side of Figure 3 contains the valence band (VB) and the conduction band (CB) spectra measured on 3 nm films of C_{60} and ZCl deposited on an indium–tin oxide (ITO) substrate. These experimental spectra are all referenced with respect to the vacuum level (VL). The experimental electronic structure can be directly interpreted using the density of states calculated for molecular C_{60} and ZCl and shown in the right side of Figure 3. From the VB spectra, a linear extrapolation of the HOMO features to the background indicates HOMO onsets for C_{60} and ZCl at -6.0 ± 0.1 and -6.4 ± 0.1 eV, respectively. A similar procedure using the CB spectra indicates that the LUMO onsets of ZCl

DOI: 10.1021/jacs.5b00146
J. Am. Chem. Soc. 2015, 137, 5397–5405

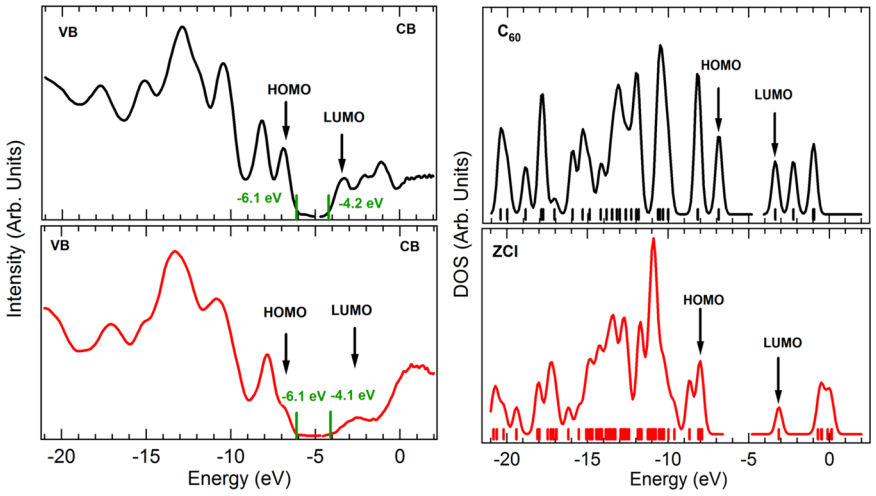

Figure 3. Left: Valence and conduction band edges of thick molecular films deposited on a DBP film. The zero of energy is the measured vacuum level of the initial DBP film. Right: Position of molecular states and resulting density of states (DOS) calculated for C_{60} and ZCl.

and C_{60} are found at -4.1 ± 0.1 and -4.2 ± 0.1 eV, respectively. The similarity of the LUMO values are in conflict with the trend in the frontier molecular orbitals derived from the reduction potentials of these materials measured previously.[25] This discrepancy could be due to stabilization in the solid state due to intermolecular interactions.[26] Additionally, the values for the LUMO of C_{60} calculated by the correlation between electrochemistry and IPS[27] deviate significantly from what has been measured independently by IPS,[28] which agree with the values measured here. The IPS values are the most relevant, as they measure the electron affinity of the solid state, the same environment seen in devices, while the electrochemistry was performed in solution. Because the LUMOs of the two acceptors are within 100 meV in energy, we expect ZCl to function as an acceptor similar to C_{60}.

To study the performance of ZCl in devices, vapor-deposited planar-heterojunction OPVs were fabricated with the structure ITO/MoO_3 (10 nm)/donor/acceptor/BCP (10 nm)/Al (100 nm), where the donor is DBP and the acceptor is either ZCl or C_{60}. The thickness of the donor layer was 20 nm and the thickness of the acceptor layer was 40 and 20 nm for devices containing C_{60} and ZCl, respectively. The device architectures, illuminated current–voltage (I–V), dark current, and external quantum efficiency (EQE) of the OPVs are given in Figure 4, and relevant parameters are given in Table 1. The DBP/ZCl device gives a power conversion efficiency (PCE) of 1.4% with J_{SC} of 2.4 mA/cm^2, V_{OC} of 1.33 V, and FF of 0.42. The DBP/C_{60} device gives a PCE of 3.6% with J_{SC} of 6.2 mA/cm^2, V_{OC} of 0.88 V, and FF of 0.68, in agreement with previous results.[23,29] The J_{SC} for the ZCl devices are lower than the C_{60} analogue due to reduced absorption between 350 and 500 nm, which is reflected in the EQE. Optical modeling using the transfer matrix formalism[30] reveals that both ZCl and DBP contribute to the photocurrent (Supporting Information, Figure S6) with an internal quantum efficiency (IQE) of approximately 30%, consistent with the estimated exciton diffusion length of 7 nm. However, the V_{OC} for the ZCl device is significantly larger. The increase in V_{OC} is also reflected in a significant reduction in dark current. Nevertheless, the PCE of the ZCl devices is less than that achieved with C_{60}. It is important to note that the goal of the present study is to determine the feasibility of using SBCT to enhance V_{OC}. As such, efficient broadband light collection, needed to achieve high PCE, was not incorporated into the devices reported here. In order to achieve a high PCE for these SBCT-based OPVs, the lack of light absorption between 350 and 550 nm can be corrected by sensitization[25,31] and the EQE values raised by shifting to an optimized bulk heterojunction, planar-mixed heterojunction, or tandem structure.[32−34]

To understand the difference in V_{OC} seen between the ZCl and C_{60} devices, it is necessary to measure the parameters that govern V_{OC}. Kinetic,[35] temperature-dependent,[13] and spectroscopic[14] treatments of V_{OC} exist, and each provides an understanding of the physics governing the generation of photovoltage in organic heterojunction systems. The temperature-dependent and spectroscopic treatments are best suited to experiment, as they contain parameters that can be independently measured. Through a detailed balance approach, E_{CT} can be related to V_{OC} by eq 1[14]

$$V_{OC} = \frac{1}{q}\left(E_{CT} + kT \ln\left(\frac{J_{SC}h^3c^2}{fq2\pi(E_{CT}-\lambda)}\right) + kT \ln(EQE_{EL})\right) \quad (1)$$

where q is the elementary charge, k is the Boltzmann constant, T is temperature, h is Planck's constant, c is the speed of light, f is proportional the CT state absorption, λ is the reorganization energy, and EQE_{EL} is the electroluminescence quantum efficiency of the CT state. The second and third terms on the right side of eq 1 correspond to the radiative (ΔV_{rad}) and nonradiative (ΔV_{nonrad}) recombination voltage losses, respectively.[14] This model has been shown to accurately predict the V_{OC} of numerous OPVs containing a variety of donors and fullerene acceptors.[13−15,36] Using this framework, we will characterize the CT state of both ZCl- and C_{60}-based devices and use the results to understand their respective V_{OC} values.

EQE spectra, measured by Fourier-transform photocurrent spectroscopy (FTPS),[37] can be seen in Figure 5a. E_{CT}, f, and λ for the devices with a DBP donor were determined from fitting the FTPS data to eq 2[14]

$$EQE \propto \frac{f}{E\sqrt{4\pi\lambda kT}} \exp\left(\frac{-(E_{CT}+\lambda-E)^2}{4\lambda kT}\right) \quad (2)$$

where geometrical reorganization, parametrized by λ, is assumed to be the origin of the Gaussian line shape of the

DOI: 10.1021/jacs.5b00146
J. Am. Chem. Soc. 2015, 137, 5397−5405

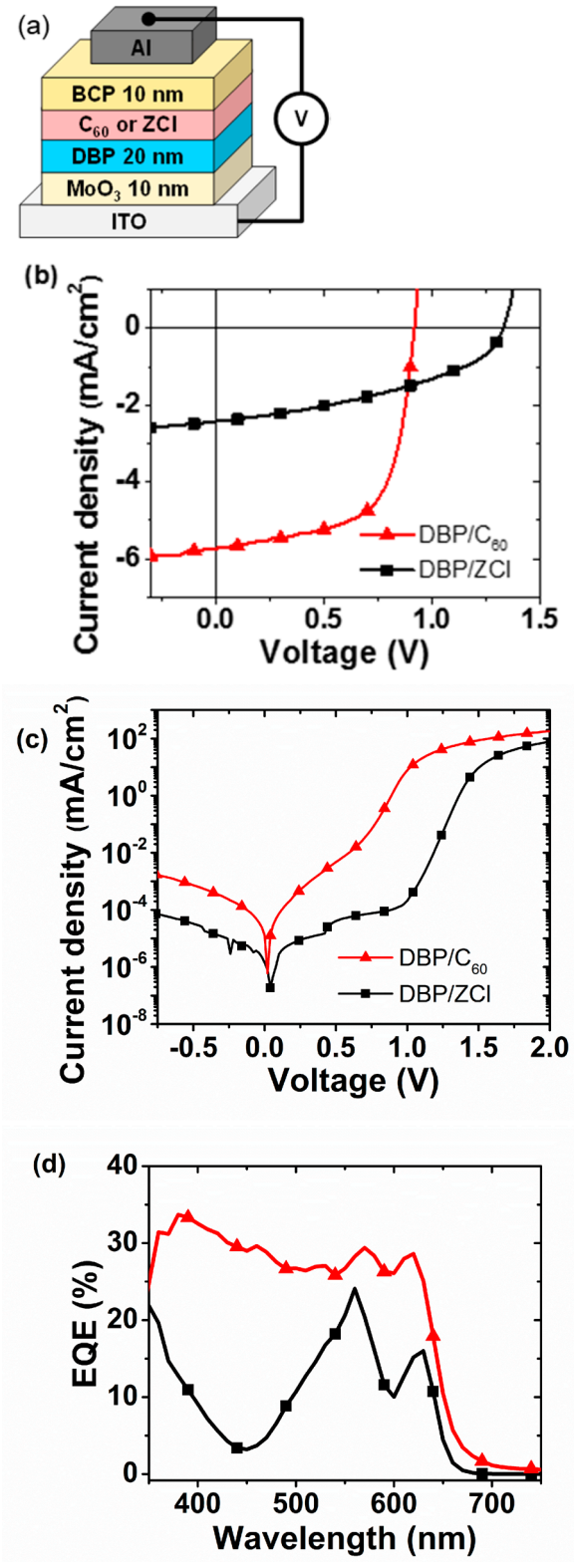

Figure 4. Device architecture (a), illuminated $I-V$ (b), dark $I-V$ (c), and EQE curves (d) for the devices described in the text. Thickness = 20 nm for DBP, 40 nm for C_{60}, and 20 nm for ZCl.

CT absorption band. In the DBP/C_{60} device E_{CT} is 1.45 ± 0.05 eV, λ is 0.242 eV, and f is 2.84×10^{-4} eV^2. The offset between the E_{CT} and qV_{OC} is 0.57 eV, ΔV_{rad} is 0.23 eV, and ΔV_{nonrad} is 0.34 eV. These results are in good agreement with previous measurements in other systems for both

Table 1. Summary of Device Performance Characteristics

device	J_{SC} (mA/cm^2)	V_{OC} (V)	FF	η (%)
DBP (20 nm)/ZCl(20 nm)	2.4	1.33	0.42	1.4
DBP (20 nm)/C_{60}(40 nm)	6.2	0.88	0.68	3.6

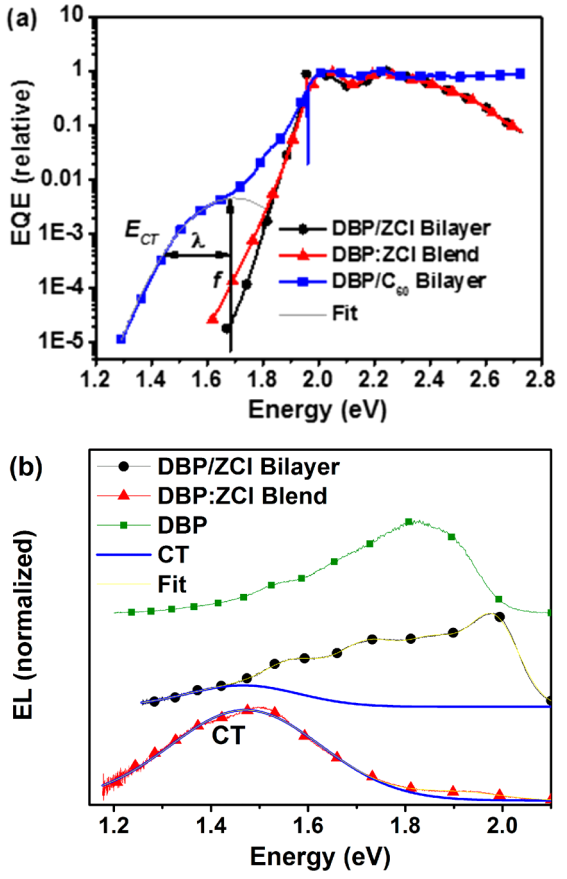

Figure 5. (a) FTPS spectra for DBP/ZCl bilayer, DBP:ZCl blend, and DBP/C_{60} bilayer devices. The lowest energy transition in the spectra for DBP:ZCl blend and DBP/C60 bilayer were fit with eq 2. (b) EL spectra for neat DBP, DBP/ZCl bilayer, and DBP:ZCl blend. The lowest energy transition in the spectra for DBP:ZCl blend and DBP/ZCl bilayer were fit with eq 3.

polymer/fullerene and small-molecule/fullerene devices.[14,15,36] In contrast, inspection of the FTPS data for the DBP/ZCl bilayer device exhibits no clear evidence of CT state absorption. This behavior could be indicative of extremely weak coupling between the donor and acceptor, or alternatively, the CT state energy could lie close to the singlet absorption of the donor, which is obscuring its detection. To increase the CT state absorption strength, allowing detection, we increased the interfacial D/A area by fabricating vacuum-deposited bulk heterojunctions (BHJs) with the structure ITO/MoO_3 (10 nm)/DBP:ZCl (40 nm)/BCP (10 nm)/Al (100 nm). There is visible enhancement in the FTPS between 1.6 and 1.8 eV, which is attributed to ground-state CT absorption; however, the signal is still too weak to perform a reliable line-shape fit.

To support the CT absorption measurements, electroluminescence (EL) measurements[38] were performed on a DBP/ZCl bilayer, DBP:ZCl BHJ, and neat DBP and are shown in Figure 5b. Both the bilayer and BHJ emission display a low-energy feature that is not present in neat DBP. Although this emission is in the same region as the ZCl triplet (λ_{max} = 1.74 eV

DOI: 10.1021/jacs.5b00146
J. Am. Chem. Soc. 2015, 137, 5397−5405

and fwhm = 0.05 eV),[25] the substantially broader line width and red-shifted intensity maximum relative to the ZCl triplet and DBP emission spectra lead us to attribute it to the CT. Because the bilayer and BHJ emission spectra display features from multiple luminescent states, the spectra were fitted with multiple Gaussian peaks. The bilayer EL exhibits contributions from DBP emission and a broad low-energy band attributed to the CT state. The BHJ EL reveals a much larger contribution from the CT state, with a weaker band attributed to DBP. Fitting the lowest energy emitting state in the EL to eq 3, analogous to that of absorption,[14]

$$\frac{I_F}{E} \propto \frac{f}{\sqrt{4\pi\lambda kT}} \exp\left(\frac{-(E_{CT} - \lambda - E)^2}{4\lambda kT}\right) \quad (3)$$

where I_F is the emission intensity, we extract E_{CT} values for the bilayer and BHJ of 1.70 ± 0.05 and 1.77 ± 0.03 eV, respectively. The CT state measurements corroborate the observed device behavior, where ZCl exhibits a larger V_{OC} than C_{60}.

The 250 meV increase in E_{CT} for the DBP/ZCl devices compared to DBP/C_{60} could be due to a number of factors. First, morphological differences between the acceptor layers in the DBP/C_{60} and DBP/ZCl devices could modify their interface with DBP, resulting in different donor−acceptor interactions. Grazing incidence X-ray diffraction measurements indicate that vapor-deposited C_{60} is polycrystalline, while ZCl is amorphous.[25] It has been shown in polymer:fullerene BHJs and bilayer small-molecule/fullerene devices that increased crystallinity of the active layer correlates with a shift in E_{CT} to lower energies, in agreement with our findings for C_{60} and ZCl.[36,39] These observations could be the result of increased delocalization of the CT state in a crystalline environment, a phenomena that has been suggested as a crucial requirement for high-efficiency OPVs.[40] Differing molecular orientation will similarly lead to changes in the electronic coupling between the donor and acceptor, as different conformations may exist at the donor/acceptor interface. This effect has been invoked to explain differences in V_{OC}, and therefore E_{CT}, seen in various systems.[41−44] Orientation dependence of electronic coupling between the donor and acceptor has also been observed in computational studies on pentacene/C_{60},[45] zinc phthalocyanine/C_{60},[43] and squaraine/C_{60}.[46] Additionally, it has been suggested that steric effects at the D/A interface can increase the energy of the CT state by increasing separation between the donor and acceptor, resulting in a higher V_{OC}.[47] However, recent studies suggest that the steric properties of the donor and/or acceptor may not be a strong contributor to the V_{OC}.[36] We hypothesize that the increase in E_{CT} is due to weak electronic coupling between donor and acceptor seen in the ZCl devices caused by incorporation of SBCT into the charge separation process. We propose that initial charge transfer occurs via SBCT and that subsequent hole transfer results in an oxidized DBP and reduced dipyrrin ligand separated by a neutral dipyrrin ligand (see Figure 1).

In conjunction with the increase in CT state energy, charge separation in the ZCl devices significantly reduces the energetic losses due to recombination from the CT state. Figure 6 shows V_{OC} as a function of E_{CT} for a variety of material systems that exhibits a linear relation with a slope of 1 and an intercept of −0.6 eV. These values are taken from Vandewal et al.,[39,48−50] Piersimoni et al.,[51] Ko et al.,[52] Hoke et al.,[7] Wang et al.,[53] Graham et al.,[36] Tietze et al.,[54] and this work. Lines with an intercept of −0.6 ± 0.1 eV are also added to show that the majority of systems fall within close proximity of this relationship. An energy difference between E_{CT} and qV_{OC} of 0.37 eV is observed for the DBP/ZCl device, which falls significantly outside the trend seen in all other systems.

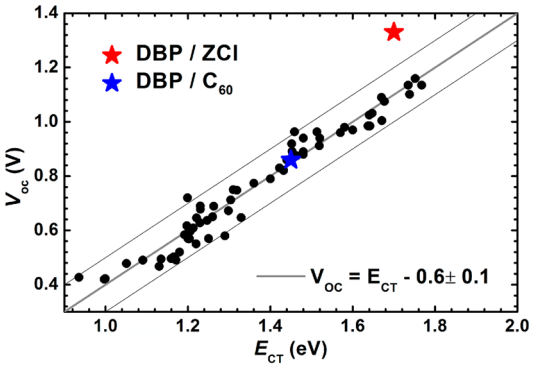

Figure 6. V_{OC} vs E_{CT} for a variety of small molecule/fullerene and polymer:fullerene OPVs. Lines at $V_{OC} = E_{CT} - 0.6 \pm 0.1$ are guides to the eye. Values are taken from Vandewal et al.,[39,48−50] Piersimoni et al.,[51] Ko et al.,[52] Hoke et al.,[7] Wang et al.,[53] Graham et al.,[36] Tietze et al.,[54] and this work.

The smaller energetic loss can be attributed to a change in the processes that govern recombination losses to V_{OC}. These losses are described above in the second and third terms of eq 1, which are catagorized as radiative and nonradiative, respectively. Due to the logarithmic dependences of these voltage losses, parameters which can only vary by less than an order of magnitude before becoming unphysical, such as J_{SC}, E_{CT}, and λ, have little effect on their size. This means that the bulk of the change in recombination losses observed between material systems is attributable to differences in f and EQE_{EL}. A weakly coupled CT state would result in a reduction of f and a corresponding decrease in recombination. Previous measurements of various devices have shown values for f between 10^{-3} and 10^{-6} eV^2,[14,36] indicative of the wide range of coupling strengths that can occur in these systems. Correspondingly, an increase in EQE_{EL} will also reduce nonradiative recombination, and values on the order of 10^{-6}−10^{-9} have been recorded for other systems.[14] In order to explain the reduction in recombination losses observed for the DBP/ZCl device, 0.37 eV as opposed to the typical 0.6 eV, there must be a factor of 10^4 change in f and EQE_{EL}. Due to the combination of weak CT absoption and emission observed for the bilayer device, we conclude that the majority of the change in recombination loss is due to a reduction in f. Overall, the recombination losses of 0.37 eV measured in the ZCl devices are equivalent to those seen in high-efficiency Si- and GaAs-based devices.[55]

The increase in E_{CT} and decrease in CT state extinction also fundamentally effect the maximum efficiency attainable in an OPV. A thermodynamic description of the efficiency limit for OPVs accounting for their excitonic nature has been formulated on the basis of a modified Shockley−Queisser analysis,[16] which describes the impact of ΔE (the energy difference between the lowest energy singlet and E_{CT}) and the CT state absorption (α_{CT}) on the highest possible efficiency for a given junction. The study concludes that at the two extremes, when ΔE or $\alpha_{CT} = 0$, the behavior of OPVs will mimic what is seen for inorganic single-juncton devices, and traditional Shockley−Queisser analysis[56] will apply. The results presented here

DOI: 10.1021/jacs.5b00146
J. Am. Chem. Soc. 2015, 137, 5397−5405

represent a significant step in this direction, as both ΔE and α_{CT} have been reduced. Further modification and optimization of the donor and acceptor energy levels in conjunction with the use of SBCT to enable efficient charge transfer with ΔE close to zero and substantially reduced coupling is an attractive strategy to bypass the fundamental limitations imposed on OPV performance.

CONCLUSION

In conclusion, we studied the photophysical and electronic properties of a non-fullerene acceptor, ZCl, and subsequently compared its performance in OPVs to that of C_{60}. SBCT was demonstrated to occur in ZCl through transient absorption studies. IPES measurements reveal that ZCl has the same LUMO as C_{60} (−4.1 eV). In OPVs, we observed that ZCl yields substantially larger V_{OC} than analogous devices with C_{60}, 1.33 V compared to 0.88 V for devices with a DBP donor. Measurements of the CT state reveal that the increase in V_{OC} originates from a combination of an increase in E_{CT} and a decrease in energetic losses due to recombination. It is proposed that these effects are related to SBCT, which substantially modulates the coupling between the donor and acceptor. In the future, we envision that SBCT materials will be particularly useful as interface materials in OPVs, where a thin layer will be placed at the D/A interface to significantly enhance V_{OC}. The results presented for ZCl are the first documented application of a material that undergoes SBCT in an OPV, and the resultant V_{OC} illustrates the great potential of this family of materials and the utilization of SBCT, in general, in OPVs. Additionally, the recombination losses from E_{CT} to V_{OC} for the DBP/ZCl devices are equivalent to what has been measured for Si and GaAs devices. Further improvement of the performance of ZCl devices, including the use of energy sensitizers to increase absorption at wavelengths shorter than 500 nm and the fabrication of optimized bulk heterojunction and tandem devices to increase photocurrent, are underway.

EXPERIMENTAL SECTION

Photophysical Characterization. Extinction coefficients for the thin films were calculated from optical constants measured by variable-angle spectroscopic ellipsometry.

Femtosecond Transient Absorption. Femtosecond pump and probe pulses were derived from the output of a Ti:sapphire regenerative amplifier (Coherent Legend, 1 kHz, 4 mJ, 35 fs). Approx. 10% of the amplifier 800 nm output was used to pump a type II optical parametric amplifier (OPA) (Spectra Physics OPA-800C) to generate a signal at ∼1540 nm and this OPA signal output was mixed with the residual 800 nm pump in a type II β-barium borate crystal to generate the 520 nm excitation pulses. At the sample position the excitation pulse is focused to ∼400 μm (fwhm) using a CaF_2 lens. White light supercontinuum probe pulses between 320 and 950 nm were obtained by focusing a small amount of the amplifier output on a rotating CaF_2 disk. The supercontinuum probe was collimated and focused with a pair of off-axis parabolic mirrors into the sample. To suppress the scattering from the excitation pulse, a perpendicularly oriented pump and probe were used to collect the data by passing the probe through an analyzing polarizer after the sample. The cross-correlation between pump and probe in a thin 1 mm quartz substrate gave a fwhm of 150 fs for 520 nm excitation. The supercontinuum probe was dispersed using a spectrograph (Oriel MS127I) onto a 256-pixel silicon diode array (Hamamatsu) for multiplexed detection of the probe.

The solutions of ZCl in cyclohexane, toluene, and acetonitrile were placed in a screw-capped 1 mm quartz cuvette. The concentration of ZCl in cyclohexane and acetonitrile was adjusted to give an optical density between 0.21 and 0.16 at 520 nm. The solutions were deaerated by bubbling with N_2 prior to analysis. The solid film of ZCl in PMMA was prepared by spin-coating on a quartz substrate to reach an optical density of 0.1 at 520 nm. The film also had an additional quartz window on the top surface, and the outer edges were sealed with epoxy under N_2 atmosphere. During data collection, the samples were slowly oscillated perpendicular to the pump and probe to reduce photodamage to the sample by the pump. Transient absorption measurements were performed with pump fluences varying between 5.7 and 40 $\mu J/cm^2$. Over this range, the signal was found to scale linearly with the pump energy.

Electron Spectroscopies. Valence and conduction band states where obtained from UV-photoemission spectroscopy (UPS) and inverse photoemission spectroscopy (IPS), respectively. The valence band spectra were measured using a He IIα line, whereas secondary electron cutoffs were obtained using a He I line, with a 5 V bias applied to the sample. Conduction band spectra were measured using a primary electron energy of 20.3 eV. The Fermi level of a gold surface in contact with the samples was used as a common energy reference for all measurements. The instrumental broadening is estimated to be 0.1 eV in UPS and 0.6 eV in IPS.

Electronic Structure. Electronic structure calculations were performed with the GAMESS(US) software package using Becke3−Lee−Yang−Parr (B3LYP) three-parameter DFT theory. Geometries of local minima on the potential energy surface were calculated with a 6-31G basis set. The density of states was obtained as a sum of the individual electronic states convoluted with a 0.47 eV full width at half-maximum Gaussian function.

OPV Fabrication and Testing. ZCl was synthesized according to published procedures.[25] DBP was obtained from Lumtec. C_{60} was obtained from MER. BCP was obtained from Sigma-Aldrich. Al (99.999%) was obtained from Alfa. All organic materials were purified by gradient sublimation before use. The devices were deposited on ITO precleaned with tergitol and organic solvents. All layers were deposited by vacuum thermal evaporation [system base pressure of $(1-3) \times 10^{-6}$ Torr] at rates between 0.02 and 0.2 nm s^{-1}. I−V measurements were performed in air at 25 °C using a Keithley 2420 Sourcemeter (sensitivity = 100 pA) in the dark and under ASTM G173-03 spectral-mismatch-corrected 1000 W/m^2 white light illumination from an AM1.5G filtered 300 W xenon arc lamp (Asahi Spectra HAL-320W). Routine spectral mismatch correction was performed using a silicon photodiode (Hamamatsu S1787-04,8RA filter) calibrated at the National Renewable Energy Laboratory (NREL). Chopped and filtered monochromatic light (250 Hz, 10 nm fwhm) from a Cornerstone 260 1/4 M double-grating monochromator (Newport 74125) was used in conjunction with an EG&G 7220 lock-in amplifier to perform all spectral responsivity and spectral mismatch correction measurements.[57]

FTPS-EQE was measured using a Nicolet iS50r FTIR with the external detector option and QTH light source, as described previously.[37] The photocurrent of the OPV of interest was amplified by a Stanford Research Systems low-noise current preamplifier. For electroluminescence measurements, solar cell devices were biased between 1.2 and 1.4 V in order to minimize the emission of pure material. An Acton Research Corp. CCD cooled to −30 °C and SpectraPro 500i spectrograph were used as the emission detection system.

ASSOCIATED CONTENT

Supporting Information

Photoluminescence quantum yield measurements of ZCl in cyclohexane, toluene, tetrahydrofuran, and acetonitrile; excited state dynamics of ZCl in different polar environments; transient absorption measurements of ZCl; global analysis of femtosecond transient absorption; kinetic model and rates extracted from transient absorption; SADS and model fits to transient absorption data; triplet sensitization of ZCl with MeI; and simulated EQE and IQE. This material is available free of charge via the Internet at http://pubs.acs.org.

DOI: 10.1021/jacs.5b00146
J. Am. Chem. Soc. 2015, 137, 5397−5405

AUTHOR INFORMATION

Corresponding Author

MET@usc.edu.

Present Address

[#]Institut für Angewandte Photophysik (IAPP), TU Dresden, 01062 Dresden, Germany.

Notes

The authors declare the following competing financial interest(s): One of the authors (M.E.T.) has a financial interest in one of the sponsors of this work (Nanoflex Power Corp.).

ACKNOWLEDGMENTS

The authors would like to acknowledge the following agencies for funding of this work: The Department of Energy, Office of Basic Energy Sciences as part of Energy Frontier Research Center program, the Center for Energy Nanoscience (DE-SC0001013, A.N.B., C.T., S.D., S.E.B.), NanoFlex Power Corp. (M.E.T.). King Abdullah University of Science and Technology (KAUST), through the Center for Molecular Photovoltaics (CAMP) is gratefully acknowledged. S.M. acknowledges support from a Stanford Graduate Fellowship. The authors also thank Bavaria California Technology Center (BaCaTeC) (M.G, W.B.). R.A.B. and S.R. were supported through grant NSF-CHE 1213727.

REFERENCES

(1) Che, X.; Xiao, X.; Zimmerman, J. D.; Fan, D.; Forrest, S. R. *Adv. Energy Mater.* **2014**, *4*, 1400568 DOI: 10.1002/aenm.201400568.

(2) You, J.; Dou, L.; Yoshimura, K.; Kato, T.; Ohya, K.; Moriarty, T.; Emery, K.; Chen, C.-C.; Gao, J.; Li, G.; Yang, Y. *Nat. Commun.* **2013**, *4*, 1446.

(3) Jorgensen, M.; Carle, J. E.; Sondergaard, R. R.; Lauritzen, M.; Dagnaes-Hansen, N. A.; Byskov, S. L.; Andersen, T. R.; Larsen-Olsen, T. T.; Bottiger, A. P. L.; Andreasen, B.; Fu, L.; Zuo, L.; Liu, Y.; Bundgaard, E.; Zhan, X.; Chen, H.; Krebs, F. C. *Sol. Energy Mater. Sol. Cells* **2013**, *119*, 84−93.

(4) Zimmerman, J. D.; Lassiter, B. E.; Xiao, X.; Sun, K.; Dolocan, A.; Gearba, R.; Vanden Bout, D. A.; Stevenson, K. J.; Wickramasinghe, P.; Thompson, M. E.; Forrest, S. R. *ACS Nano* **2013**, *7*, 9268−9275.

(5) Lin, Y.; Li, Y.; Zhan, X. *Chem. Soc. Rev.* **2012**, *41*, 4245−4272.

(6) Bijleveld, J. C.; Verstrijden, R. A. M.; Wienk, M. M.; Janssen, R. A. J. *Appl. Phys. Lett.* **2010**, *97*, 073304.

(7) Hoke, E. T.; Vandewal, K.; Bartelt, J. A.; Mateker, W. R.; Douglas, J. D.; Noriega, R.; Graham, K. R.; Fréchet, J. M. J.; Salleo, A.; McGehee, M. D. *Adv. Energy Mater.* **2012**, *3*, 220−230.

(8) Sonar, P.; Fong Lim, J. P.; Chan, K. L. *Energy Environ. Sci.* **2011**, *4*, 1558−1574.

(9) Facchetti, A. *Mater. Today* **2013**, *16*, 123−132.

(10) Cnops, K.; Rand, B. P.; Cheyns, D.; Verreet, B.; Empl, M. A.; Heremans, P. *Nat. Commun.* **2014**, *5*, 3406 DOI: 10.1038/ncomms4406.

(11) Sullivan, P.; Duraud, A.; Hancox, l.; Beaumont, N.; Mirri, G.; Tucker, J. H. R.; Hatton, R. A.; Shipman, M.; Jones, T. S. *Adv. Energy Mater.* **2011**, *1*, 352−355.

(12) Peng, Y.; Zhang, L.; Andrew, T. L. *Appl. Phys. Lett.* **2014**, *105*, 083304.

(13) Hormann, U.; Kraus, J.; Gruber, M.; Schuhmair, C.; Linderl, T.; Grob, S.; Kapfinger, S.; Klein, K.; Stutzman, M.; Krenner, H. J.; Brutting, W. *Phys. Rev. B* **2013**, *88*, 235307.

(14) Vandewal, K.; Tvingstedt, K.; Gadisa, A.; Inganas, O.; Manca, J. V. *Phys. Rev. B* **2010**, *81*, 125204.

(15) Widmer, J.; Tietze, M.; Leo, K.; Riede, M. *Adv. Funct. Mater.* **2013**, *23*, 5814−5821.

(16) Gruber, M.; Wagner, J.; Klein, K.; Hörmann, U.; Opitz, A.; Stutzmann, M.; Brütting, W. *Adv. Energy Mater.* **2012**, *2*, 1100−1108.

(17) Grabowski, Z. R.; Rotkiewicz, K.; Rettig, W. *Chem. Rev.* **2003**, *103*, 3899−4032.

(18) Rettig, W. *Angew. Chem. Int. Ed. Engl.* **1986**, *25*, 971−988.

(19) Schneider, F.; Lippert, E. *Ber. Bunsen-Ges.* **1968**, *72*, 1155−1160.

(20) Wasielewski, M. R. *Acc. Chem. Res.* **2009**, *42*, 1910−1921.

(21) Giaimo, J. M.; Gusev, A. V.; Wasielewski, M. R. *J. Am. Chem. Soc.* **2002**, *124*, 8530−8531.

(22) Trinh, C.; Kirlikovali, K. O.; Das, S.; Ener, M. E.; Gray, H. B.; Djurovich, P. I.; Bradforth, S.; Thompson, M. E. *J. Phys. Chem. C* **2014**, *118*, 21834−21845.

(23) Yokoyama, D.; Qiang Wang, Z.; Pu, Y.-J.; Kobayashi, K.; Kido, J.; Hong, Z. *Sol. Energy Mater. Sol. Cells* **2012**, *98*, 472−475.

(24) Kazaoui, S.; Minami, N.; Tanabe, Y.; Byrne, H. J.; Eilmes, A.; Petelenz, P. *Phys. Rev. B* **1998**, *58*, 7689−7700.

(25) Trinh, C.; Kirlikovali, K. O.; Bartynski, A. N.; Tassone, C. J.; Toney, M. F.; Burkhard, G. F.; McGehee, M. D.; Djurovich, P. I.; Thompson, M. E. *J. Am. Chem. Soc.* **2013**, *135*, 11920−11928.

(26) Sweetnam, S.; Graham, K. R.; Ngongang Ndjawa, G. O.; Heumuller, T.; Bartelt, J. A.; Burke, T. M.; Li, W.; You, W.; Amassian, A.; McGehee, M. D. *J. Am. Chem. Soc.* **2014**, *136*, 14078−14088.

(27) Djurovich, P. I.; Mayo, E. I.; Forrest, S. R.; Thompson, M. E. *Org. Electron.* **2009**, *10*, 515−520.

(28) Wilke, A.; Endres, J.; Hormann, U.; Niederhausen, J.; Schlesinger, R.; Frisch, J.; Amsalem, P.; Wagner, J.; Gruber, M.; Opitz, A.; Vollmer, A.; Brutting, W.; Kahn, A.; Koch, N. *Appl. Phys. Lett.* **2012**, *101*, 233301.

(29) Fujishima, D.; Kanno, H.; Kinoshita, T.; Maruyama, E.; Tanaka, M.; Shirakawa, M.; Shibata, K. *Sol. Energy Mater. Sol. Cells* **2009**, *93*, 1029−1032.

(30) Pettersson, L. A. A.; Roman, L. S.; Inganas, O. *J. Appl. Phys.* **1999**, *86*, 487−496.

(31) Bartynski, A. N.; Trinh, C.; Kirlikovali, K. O.; Thompson, M. E. *Appl. Phys. Lett.* **2014**, *105*, 113305.

(32) Che, X.; Xiao, X.; Zimmerman, J. D.; Fan, D.; Forrest, S. R. *Adv. Energy Mater.* **2014**, *4*, 1400568 DOI: 10.1002/aenm.201400568.

(33) Xue, J.; Rand, B. P.; Uchida, S.; Forrest, S. R. *Adv. Mater.* **2005**, *17*, 66−71.

(34) Peumans, P.; Uchida, S.; Forrest, S. R. *Nature* **2003**, *425*, 158−162.

(35) Giebink, N. C.; Wiederrecht, G. P.; Wasielewski, M. R.; Forrest, S. R. *Phys. Rev. B* **2010**, *82*, 155305.

(36) Graham, K. R.; Erwin, P.; Nordlund, D.; Vandewal, K.; Li, R.; Ngongang Ndjawa, G. O.; Hoke, E. T.; Salleo, A.; Thompson, M. E.; McGehee, M. D.; Amassian, A. *Adv. Mater.* **2013**, *25*, 6076−6082.

(37) Vandewal, K.; Goris, L.; Haeldermans, I.; Nesladek, M.; Haenen, K.; Wagner, P.; Manca, J. V. *Thin Solid Films* **2008**, *516*, 7135−7138.

(38) Tvingstedt, K.; Vandewal, K.; Gadisa, A.; Zhang, F.; Manca, J.; Inganas, O. *J. Am. Chem. Soc.* **2009**, *131*, 11819−11824.

(39) Vandewal, K.; Gadisa, A.; Oosterbaan, W. D.; Bertho, S.; Banishoeib, F.; Van Severen, I.; Lutsen, L.; Cleij, T. J.; Vanderzande, D.; Manca, J. V. *Adv. Funct. Mater.* **2008**, *18*, 2064−2070.

(40) Savoie, B. M.; Rao, A.; Bakulin, A. A.; Gelinas, S.; Movaghar, B.; Friend, R. H.; Marks, T. J.; Ratner, M. A. *J. Am. Chem. Soc.* **2014**, *136*, 2876−2884.

(41) Perez, M. D.; Borek, C.; Forrest, S. R.; Thompson, M. E. *J. Am. Chem. Soc.* **2009**, *131*, 9281−9286.

(42) Yamamoto, S.; Orimo, A.; Ohkita, H.; Benten, H.; Ito, S. *Adv. Energy Mater.* **2011**, *2*, 229−237.

(43) Rand, B. P.; Cheyns, D.; Vasseur, K.; Giebink, N. C.; Mothy, S.; Yi, Y.; Coropceanu, V.; Beljonne, D.; Cornil, J.; Brédas, J.-L.; Genoe, J. *Adv. Funct. Mater.* **2012**, *22*, 2987−2995.

(44) Erwin, P.; Thompson, M. E. *Appl. Phys. Lett.* **2011**, *98*, 223305.

(45) Yi, Y.; Coropceanu, V.; Bredas, J.-L. *J. Am. Chem. Soc.* **2009**, *131*, 15777−15783.

(46) Fu, Y.-T.; da Silva Filho, D. A.; Sini, G.; Asiri, A. M.; Aziz, S. G.; Risko, C.; Brédas, J.-L. *Adv. Funct. Mater.* **2014**, *24*, 3790−3798.

(47) Holcombe, T. W.; Norton, J. E.; Rivnay, J.; Woo, C. H.; Goris, L.; Piliego, C.; Griffini, G.; Sellinger, A.; Bredas, J.-L.; Salleo, A.; Frechet, J. M. J. *J. Am. Chem. Soc.* **2011**, *133*, 12106−12114.

DOI: 10.1021/jacs.5b00146
J. Am. Chem. Soc. 2015, 137, 5397−5405

(48) Vandewal, K.; Tvingstedt, K.; Gadisa, A.; Inganas, O.; Manca, J. V. *Nat. Mater.* **2009**, *8*, 904−909.
(49) Vandewal, K.; Widmer, J.; Heumueller, T.; Brabec, C. J.; McGehee, M. D.; Leo, K.; Riede, M.; Salleo, A. *Adv. Mater.* **2014**, *26*, 3839−3843.
(50) Vandewal, K.; Oosterbaan, W. D.; Bertho, S.; Vrindts, V.; Gadisa, A.; Lutsen, L.; Vanderzande, D.; Manca, J. V. *Appl. Phys. Lett.* **2009**, *95*, 123303.
(51) Piersimoni, F.; Chambon, S.; Vandewal, K.; Mens, R.; Boonen, T.; Gadisa, A.; Izquierdo, M.; Filippone, S.; Ruttens, B.; D'Haen, J.; Martin, N.; Lutsen, L.; Vanderzande, D.; Adriaensens, P.; Manca, J. V. *J. Phys. Chem. C* **2011**, *115*, 10873−10880.
(52) Ko, S.; Hoke, E. T.; Pandey, L.; Hong, S.; Mondal, R.; Risko, C.; Yi, Y.; Noriega, R.; McGehee, M. D.; Bredas, J.-L.; Salleo, A.; Bao, Z. *J. Am. Chem. Soc.* **2012**, *134*, 5222−5232.
(53) Wang, E.; Bergqvist, J.; Vandewal, K.; Ma, Z.; Hou, L.; Lundin, A.; Himmelberger, S.; Salleo, A.; Müller, C.; Inganäs, O.; Zhang, F.; Andersson, M. R. *Adv. Energy Mater.* **2013**, *3*, 806−814.
(54) Tietze, M.; Tress, W.; Pfatzner, S.; Schanemann, C.; Burtone, L.; Riede, M.; Leo, K.; Vandewal, K.; Olthof, S.; Schulz, P.; Kahn, A. *Phys. Rev. B* **2013**, *88*, 085119.
(55) King, R. R.; Bhusari, D.; Boca, A.; Larrabee, D.; Liu, X. Q.; Hong, W.; Fetzer, C. M.; Law, D. C.; Karam, N. H. *Prog. Photovoltaics* **2011**, *19*, 797−812.
(56) Shockley, W.; Queisser, H. J. *J. Appl. Phys.* **1961**, *32*, 510−519.
(57) Seaman, C. H. *Sol. Energy* **1982**, *29*, 291−298.

DOI: 10.1021/jacs.5b00146
J. Am. Chem. Soc. 2015, 137, 5397−5405